Fast Estimation of Intrinsic Volumes in 3D Gray Value Images

Michael Godehardt(✉), Andreas Jablonski, Oliver Wirjadi, and Katja Schladitz

Fraunhofer-Institut für Techno- und Wirtschaftsmathematik,
D-67663 Fraunhofer-Platz 1, Kaiserslautern, Germany
michael.godehardt@itwm.fraunhofer.de
www.itwm.fraunhofer.de/en/departments/image-processing/

Abstract. The intrinsic volumes or their densities are versatile structural characteristics that can be estimated efficiently from digital image data, given a segmentation yielding the structural component of interest as foreground. In this contribution, Ohser's algorithm is generalized to operate on integer gray value images. The new algorithm derives the intrinsic volumes for each possible global gray value threshold in the image. It is highly efficient since it collects all neccesary structural information in a single pass through the image.

The novel algorithm is well suited for computing the Minkowski functions of the parallel body if combined with the Euclidean distance transformation. This application scenario is demonstrated by means of computed tomography image data of polar ice samples. Moreover, the algorithm is applied to the problem of threshold selection in computed tomography images of material microstructures.

Keywords: Intrinsic volumes · Gray value images · Minkowsi functions · Connectivity analysis · Segmentation · Microstructure analysis

1 Introduction

The possibilites and the demand to spatially image materials microstructures has grown tremendiously during the last decade. Image sizes, complexity of the imaged structures, and detail of the analysis tasks grow at even higher speed, increasing the demand for time and memory efficient algorithms yielding quantitative structural information.

One very general image analysis tool are the intrinsic volumes. The intrinsic volumes, also known as Minkowski functionals or quermass integrals [1], are in some sense a basic set of geometric structural characteristics [2]. In 3D, they yield information about the volume, surface, mean and Gaussian curvatures of analyzed structures. Various other characteristics describing e.g. shape [3] or structure specific features e. g. for open cell foams [4] can be derived. The densities of the intrinsic volumes, combined with erosions and dilations of the structure under consideration have been studied, e. g. to quantify connectivity [5]. Mecke [6] called them Minkowski functions.

J.A. Benediktsson et al. (Eds.): ISMM 2015, LNCS 9082, pp. 657–668, 2015.
DOI: 10.1007/978-3-319-18720-4_55

For a given segmentation of the gray value image into the component of interest (foreground) and its complement (background), the intrinsic volumes can be efficiently derived from the resulting binary image by Ohser's algorithm [7,8]. In this paper, we generalize Ohser's approach to gray value images. That is, we introduce an algorithm for fast simultaneous calculation of the intrinsic volumes for all possible threshold values in an integer gray value image.

The usefulness of the new algorithm is proved by applying it to X-ray computed tomography images of materials microstructures: In the first scenario, we apply our new algorithm to the Euclidean distance transformed image. This yields immediately the Minkowski functions widely used in physical applications [6]. For polar ice, they reveal structural differences of the multiply connected pore system.

In the second scenario, we exploit our new algorithm to find the optimal global gray value threshold: Segmentation remains a notorius problem, even in the simplest case of porous materials consisting of one homogeneous solid component with a clear contrast to the air filled pore space. Identification of the solid phase in the image data is an essential prerequisite for the majority of geometric analyses as well as for numerical simulation of macroscopic materials properties using the segmented image data as computational domain. In engineering, fast, objective segmentation methods are sought after. Global gray value thresholding is the easiest choice and competes well as long as global gray value fluctuations have been avoided or removed. It remains to devise a strategy to determine the threshold. There is a variety of threshold selection schemes, most prominent Otsu's [9] and the isodata method [10].

Here, we pursue the obvious idea of choosing the threshold such that previously known characteristics of the imaged structure are met. Examples for such characteristics range from simple prior knowledge such as the solid volume fraction of the component of interest to more complex properties of microstructures such as surface density or mean thickness. Of course, this approach is endangered by noise, porosity on a scale finer than the image resolution and imaging artefacts. Discretization effects further complicate matters, in the case of X-ray computed tomography in particular the partial volume effect. Nevertheless, one could hope for a range of possible thresholds, where essential geometric characteristics do not change drastically. This could be identified by monitoring the dependence of these characteristics on the gray value threshold. This idea is pursued for a glass fiber reinforced composite.

2 Estimation of Intrinsic Volumes in 3D Binary Images

The intrinsic volumes (or their densities) are a system of basic geometric characteristics for microstructures. In 3D, there are four intrinsic volumes – the volume V, the surface area S, the integral of mean curvature M and the Euler number χ. For a convex object, M is up to a constant the mean width. The Euler number is a topological characteristic alternately counting the connected components, the tunnels, and the holes. For a convex body, we have $\chi = 1$, for a

torus $\chi = 1 - 1 = 0$, and for a sphere $\chi = 1 + 1 = 2$. For macroscopically homogeneous structures, the densities of the intrinsic volumes are considered instead – the volume fraction V_V, the specific surface area S_V, the density of the integral of mean curvature M_V, and the density of the Euler number χ_V. That is, the respective quantities are divided by the total sample volume measured. These characteristics can be estimated based on observations restricted to a compact window.

An efficient algorithm for the simultaneous measurement of all intrinsic volumes from 3D image data is based on weighted local $2 \times 2 \times 2$ pixel configurations in a binary 3D image [8, Chapter 5]. The restriction to these small configurations allows to code them in an 8bit gray value image of the same size using the convolution with the mask shown in Figure 1. All further steps of the algorithm are based solely on the gray value histogram h of this image whose size does not depend on image size or content. Thus it is simple and fast to compute the intrinsic volumes. The algorithm is deduced from a discrete version of the

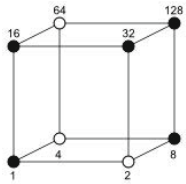

Fig. 1. Mask used for coding the $2 \times 2 \times 2$ pixel configurations. Here, the black colored pixels are set resulting in configuration code $c(p) = 182$

integral geometric Crofton formulae [8,11] boiling down computing the intrinsic volumes to computing Euler numbers in lower dimensional intersections. The Euler numbers in turn can be estimated efficiently in the discrete setting by the Euler-Poincaré formula as the alternating sum of numbers of cells, faces, edges, and vertices. We shortly summarize the algorithm:

1. Given the 3D image of a microstructure, binarize it, e. g. using a global gray value threshold.
2. Convolve the binary image with the following $2 \times 2 \times 2$ mask:

$$\left(\begin{pmatrix} 1 & 2 \\ 4 & 8 \end{pmatrix}, \begin{pmatrix} 16 & 32 \\ 64 & 128 \end{pmatrix} \right). \tag{1}$$

3. Compute the gray value histogram h of the convolution result.
4. Calculate the intrinsic volumes as scalar products of h with tabulated weight vectors $v^{(k)}$, $k = 0, \ldots, 3$ derived from discretizing the Crofton formulae, [8, Section 5.3.5].

Note that the specific choice of a weight vector v in step 4 depends on the discrete connectivities assumed for foreground and background of the image.

3 Estimation of Intrinsic Volumes as Function of Gray Value Threshold

In this section, we generalize the algorithm sketched in the previous section to gray value images. As before, the actual calculation of the intrinsic volumes consists of scalar multiplication of suitable weight vectors with the vector h of frequencies of $2 \times 2 \times 2$ black-or-white pixel configurations. The generalization is achieved by an algorithm for efficiently collecting and coding the local black-or-white pixel configurations induced by thresholding the local pixel configurations in gray value images.

The naive generalization of the algorithm from Section 2 would loop through the image's gray value range $R = \{0, \ldots, 255\}$ for 8bit gray values or $R = \{0, \ldots, 2^{16} - 1\}$ for 16bit gray values, use each value $t \in R$ as global gray value threshold, and apply the algorithm sketched above to each of the resulting binary images. Clearly, this is not practical. Instead, the matrix of the frequency vectors $h(t), t \in R$, is created and exploited. The main observation yielding an efficient algorithm is the following: For each local $2 \times 2 \times 2$ pixel configuration $p = (p_1, \ldots, p_8)$, only those eight pixels' gray values are threshold values, for which the contribution of p changes. Here, thresholding with $t \geq 0$ means the following: The gray value of pixel p_i is set to 1 if it was larger or equal to t and to 0 else.

Before describing details of the algorithm, we introduce some notation: Let $M = \max\{R\}$ be the maximal gray value in the image. Write $c(p, t)$ for the code of pixel configuration p after thresholding with threshold t. Without loss of generality, we assume the structures of interest to be represented by bright values, i.e., with larger gray values. Then, in particular, $c(p, 0) = 255$ and $c(p, M+1) = 0$ for all p as thresholding by 0 creates the configuration completely contained in the foreground and thresholding by more than the maximal possible gray value creates the configuration completely contained in the background. For all remaining threshold values, $c(p, t)$ represents the result of the convolution with the mask from (1) if the image has been thresholded at t.

1. All changes are stored in the difference matrix $\Delta(c, t)$, $c = 0, \ldots, 255$, $t = 0, \ldots, M + 1$ initialized with 0.
2. For local pixel configuration p do
   (a) Sort the current eight gray values $t_1, \ldots, t_8$ and let $0 = t_0 \leq t_1 \leq \ldots \leq t_8 \leq M$.
   (b) For $i = 0, \ldots, 7$ do
      – Increase $\Delta(c(p, t_i), t_i + 1)$ by one.
      – Decrease $\Delta(c(p, t_i), t_{i+1} + 1)$ by one.
   (c) Increase $\Delta(0, t_8 + 1)$ by one.
3. Initialize the final matrix h by $h(c, t) = 0$ for all $c \in \{0, \ldots, 255\}$, $t \in \{0, \ldots, M + 1\}$.
4. $h(c, t) = \sum_{\tau=0}^{t} \Delta(c, \tau)$.

This results in $h(\cdot, t)$ being the configuration frequency vector for the image thresholded at t. Note that in general, for d-dimensional images, $\Delta(c, t)$ has

$2^{2^d} \times M + 1$ elements, independent of the actual size of the image. E.g., for the case of 3D 8bit gray value images, this amounts to a memory requirement of $256 \cdot 256 = 65536$ integers to process any such image, regardless of its size.

Example 1. For the sake of clarity and brevity of the presentation, we just consider a 2D 8bit gray value image, that is, the 2×2 configurations are coded by convolution with

$$\begin{pmatrix} 1 & 2 \\ 4 & 8 \end{pmatrix}$$

and the difference matrix $\Delta(c,t)$ has dimensions 16×256. In the 2D case, $c(p,0) = 1+2+4+8 = 15$ and $c(p,256) = 0$ for all p. Let the image consist of just one 2×2 pixel configuration

$$\begin{pmatrix} 26 & 4 \\ 128 & 17 \end{pmatrix}.$$

Sorting yields $t_1 = 4,\ t_2 = 17,\ t_3 = 26,\ t_4 = 128$. Now the algorithm proceeds as follows

1. Increase $\Delta(15,0)$ by one. Decrease $\Delta(15,5)$ by one.
2. Binarization with threshold $t_1 = 4$ yields the configuration

   $$\begin{pmatrix} 1 & 0 \\ 1 & 1 \end{pmatrix}$$

   whose code is $1+4+8 = 13$. Thus increase $\Delta(13,5)$ by one. Decrease $\Delta(13,18)$ by one.
3. Binarization with threshold $t_2 = 17$ yields the configuration

   $$\begin{pmatrix} 1 & 0 \\ 1 & 0 \end{pmatrix}$$

   whose code is $1+4 = 5$. Thus increase $\Delta(5,18)$ by one. Decrease $\Delta(5,27)$ by one.
4. Binarization with threshold $t_3 = 26$ yields the configuration

   $$\begin{pmatrix} 0 & 0 \\ 1 & 0 \end{pmatrix}$$

   whose code is 4. Thus increase $\Delta(4,27)$ by one. Decrease $\Delta(4,129)$ by one.
5. Binarization with threshold $t_4 = 128$ yields the configuration

   $$\begin{pmatrix} 0 & 0 \\ 0 & 0 \end{pmatrix}$$

   whose code is 0. Thus increase $\Delta(0,129)$ by one.

This results in

$$\Delta(c,t) = \begin{array}{c} \\ 0 \\ \vdots \\ 4 \\ 5 \\ \vdots \\ 13 \\ \vdots \\ 15 \end{array} \begin{array}{c} \begin{array}{ccccccccccc} 0 & \cdots & 5 & \cdots & 18 & \cdots & 27 & \cdots & 129 & \cdots & 256 \end{array} \\ \begin{pmatrix} 0 & \cdots & 0 & \cdots & 0 & \cdots & 0 & \cdots & 1 & \cdots & 0 \\ \\ 0 & \cdots & 0 & \cdots & 0 & \cdots & 1 & \cdots & -1 & \cdots & 0 \\ 0 & \cdots & 0 & \cdots & 1 & \cdots & -1 & \cdots & 0 & \cdots & 0 \\ \\ 0 & \cdots & 1 & \cdots & -1 & \cdots & 0 & \cdots & 0 & \cdots & 0 \\ \\ 1 & \cdots & -1 & \cdots & 0 & \cdots & 0 & \cdots & 0 & \cdots & 0 \end{pmatrix} \end{array}$$

Summing up yields $h(\cdot,t) = (0,\ldots,0,1)$ for $t = 0,\ldots,4$. Then, the configuration changes and thus $h(\cdot,t) = (\underbrace{0,\ldots,0}_{13\text{times}},1,0,0)$ for $t = 5,\ldots,17$. At threshold 18 the next change happens, resulting in $h(\cdot,t) = (0,0,0,0,0,1,0,\ldots,0)$ for $t = 18,\ldots,26$. The configuration changes next at threshold 27 and yields $h(\cdot,t) = (0,0,0,0,1,0,\ldots,0)$ for $t = 27,\ldots,128$. Finally $h(\cdot,t) = (1,0,\ldots,0)$ for $t = 129,\ldots,256$.

4 Application Examples

In the following, the just derived algorithm is applied to two real 3D images of microstructures. For the pore system in polar ice samples from two different depths, the densities of the intrinsic volumes with respect to dilations and erosions are derived, revealing structural differences. For a glass fiber reinforced composite, a suitable global gray value threshold is found using prior knowledge on the imaged structure.

4.1 Polar Firn: Erosion-Dilation Analysis

Polar ice is a climate information archive and therefore of considerable interest for climate research. During the last decades a couple of deep polar ice cores were drilled through the Antarctic and Greenlandic ice sheets. The upper 50 to 100m of these ice sheets are formed by so-called firn – sintered ice grains with an inter-connected air-filled pore system. Here, we consider samples of firn core B26 drilled during the the North-Greenland-Traverse in 1993-1995 from depths between 56m and 72m, first studied in [12]. Volume renderings are shown in Figure 2.

The Minkowski functions as used e.g. in [6] are the intrinsic volumes of parallel body $X \oplus B_r$ resp. $X \ominus B_r$ of the structure X over the radius r, that is, the intrinsic volumes of stepwise erosions/dilations of X. From these functions, 3d structural information can be directly derived. In particular the specific Euler number as a function of successive erosions was called connectivity function

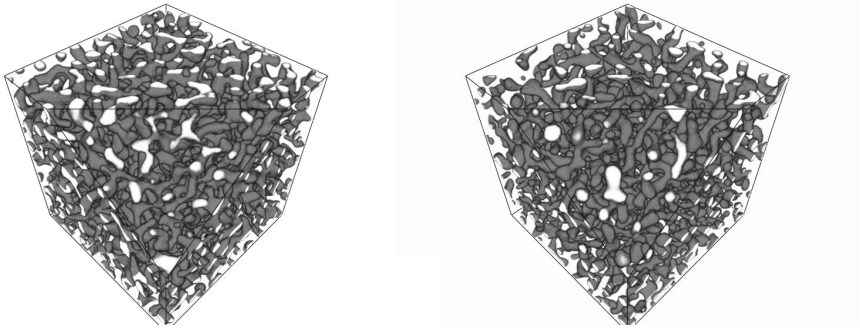

(a) Sample from depth 56m. **(b)** Sample from depth 72m.

Fig. 2. Volume rendering of the pore system of firn core B26 from North Greenland. Pixel edge length 40μm, visualized are $400 \times 400 \times 400$ pixels corresponding to 16mm $\times$ 16mm $\times$ 16mm

and used to evaluate bond sizes [5]. In [13], the Euler number combined with successive erosions was used to study the connectivity of firn from the B35 core, see also [8].

Here, we exploit the algorithm derived in 3 and the fact that erosions and dilations with a ball can be efficently computed via thresholding the result of the Euclidean distance transformation (EDT). That is, the Minkowski functions are computed using the novel algorithm on the EDT image. Edge effects are avoided by minus-sampling the distance images. Figure 3 shows the results for

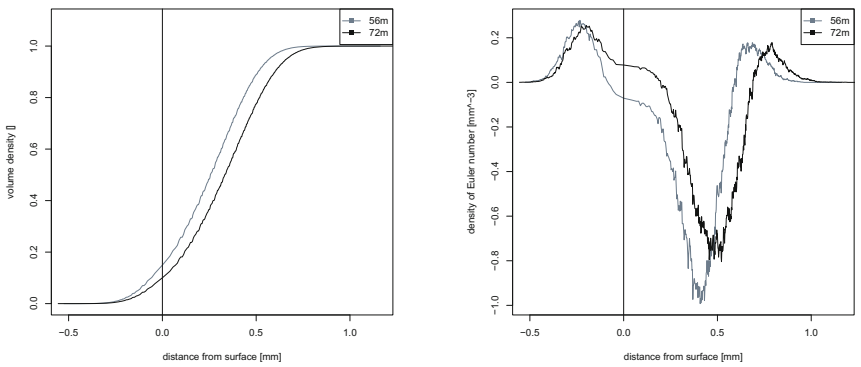

(a) Volume density function **(b)** Euler number density function

Fig. 3. Minkowski functions (a) $V_V(X \ominus B_r)$ and $V_V(X \oplus B_r)$, and (b) $\chi_V(X \ominus B_r)$ and $\chi_V(X \oplus B_r)$, where X denotes the pore system of the firn sample. That means, negative distances correspond to erosions of the pore system or dilations of the ice, while positive distances correspond to dilations of the pore system or erosions of the ice.

the volume fraction and the Euler number density, both applied to the pore system.

First, obviously, in the deeper sample the porosity is sligtly smaller. This can be seen from the volume densities for negative distances in Fig. 3a, where the porosity in the deeper sample (72m) vanishes in earlier erosion steps of the pore space than in case of 56m.

Recall that isolated pores contribute positively to the Euler number. The Euler number density of the original pore system in the 72m sample is positive, indicating a prevelance of isolated pores, while the Euler number density of the pore system in the 56m sample is negative as the pore system is more strongly connected (Fig. 3b).

Looking at the maxima of the Euler number densities in both samples for negative distances, we see that connections between pores are broken by smaller erosions of the pore space at 72m than at 56m. In other words, the inter-pore connections appear to be thinner in the lower sample.

The minimum of the Euler number density is reached later for the 72m sample, showing that the ice grains are isolated in a later dilation step. This indicates locally thicker ice grains in the deeper sample, ie., larger pore-to-pore distances.

These findings are consistent with the findings in earlier studies of such systems [12,14,15].

4.2 Glass Fiber Reinforced Composite: Surface Density-Based Threshold Selection

Here, we briefly summarize an algorithm for threshold selection which incorporates prior knowledge exploiting the efficiency of the fast estimation of intrinsic volumes for gray valued data that was proposed in this paper. First, observe that due to the Steiner formula, for a sufficiently smooth bounded set X we have

$$\lim_{r\to 0}(V_V(X \oplus B_r) - V_V(X))/r = \frac{dV_V}{dr}(X) = S_V(X). \tag{2}$$

For a rigourous derivation see [2, Section 14.4] or [3].

Moreover, observe that roughly, decreasing or increasing the threshold slightly is equivalent to a dilation or erosion, respectively. Thus, dV_V/dt, where t denotes the gray value threshold, can be interpreted as an estimator for the specific surface area S_V.

However, our experiments have shown that this estimator is far too sensitive to noise and discretization effects in order to yield a reliable result for S_V. This relation can nevertheless be successfully exploited in order to find a good gray value threshold. To this end, our surface density-based threshold selection scheme exploits that $S_V(X(t))/(dV_V(X(t))/dt) = 1$, where $X(t)$ denotes the foreground set induced through applying threshold t to the input image, when we assume that Δt gets infinitesimally small. Thus, we may choose t such that this condition will be fulfilled. The rationale behind it is that if the foreground structures depicted in some gray value image fulfill the prerequisites of the Steiner formula, the ratio should approach one for the correct threshold. Wrong thresholds, on

the other hand, are expected to destroy the structure (e.g. due to noise), thus invalidating that ratio.

Given a 3D image, we implement that idea in the following algorithm.

1. Compute the intrinsic volumes of the image for all thresholds t using the algorithm from above.
2. Apply a backward difference filter on this result to obtain $dV_V(X(t))/dt$.
3. Choose the mode of the ratio of $S_V(X(t))$ and $dV_V(X(t))/dt$ to obtain the surface density-based threshold.

The third and last step of this algorithm is particularly important. First note, that we cannot get an infinitesimally small ball B_r, but we have a difference quotient in the second step. Therefore, there are remaining terms in the Steiner formulae, so the ratio may not reach one. So we choose instead the mode of the ratio. This is necessary since for real data, discretization effects have a major impact on the results. E.g., increasing the threshold by one can result in quite strong erosions, thus violating equation 2, where the dilation should be with an infinitesimally small structuring element.

Nevertheless, we observe that in practice, there will be a pronounced peak in $S_V(X(t))/(dV_V(X(t))/dt)$. This phenomenon is caused by the contrast of the images, which should always be highest around the structures under investigation. Thus, $dV_V(X(t))/dt$ can be expected to be low at the threshold value of interest, while $S_V(X(t))$ should approach the true value of $S_V(X)$ at that point.

We finally consider a glass fiber reinforced polymer sample, more precisely a polypropylene matrix reinforced by long glass fibers (average length of 7 mm, diameter of about 16 μm). The sample of size $6 \times 4 \times 6$ mm^3 was imaged by X-ray computed tomography with a pixel edge length of 4 μm. For details on sample production parameters and μCT imaging see [16], where the local fiber orientations were analyzed in order to identify the misoriented region in the central part.

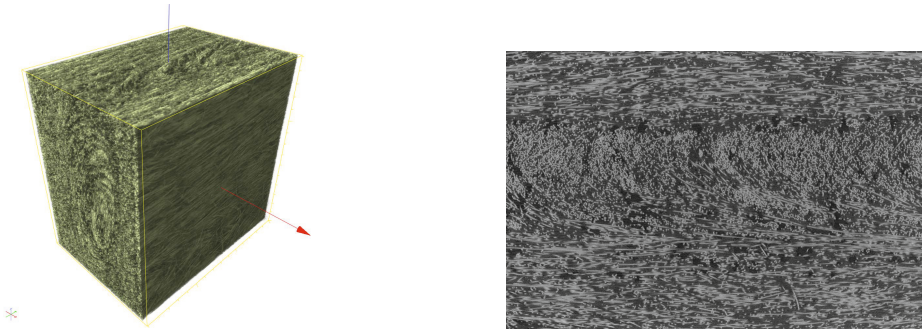

(a) Volume rendering **(b)** Slice view

Fig. 4. Volume rendering of and section through the glass fiber reinforced polymer sample. Sample preparation and μCT imaging IVW Kaiserslautern. Pixel edge length 4 μm. Visualized are $1\,100 \times 1\,500 \times 1\,500$ pixels corresponding to 4mm $\times$ 6mm $\times$ 6mm.

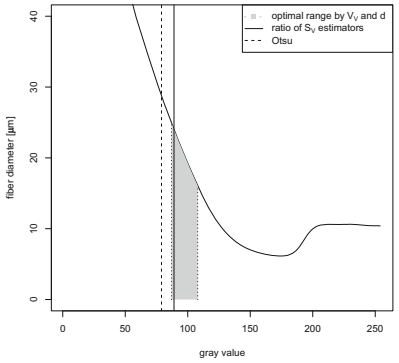

(a) Mean fiber diameter

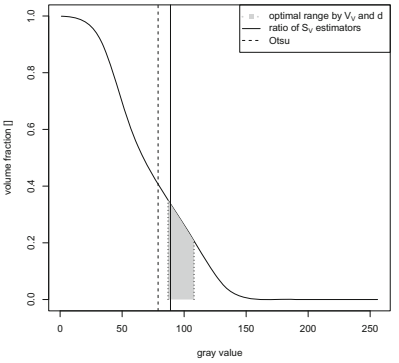

(b) Fiber volume fraction

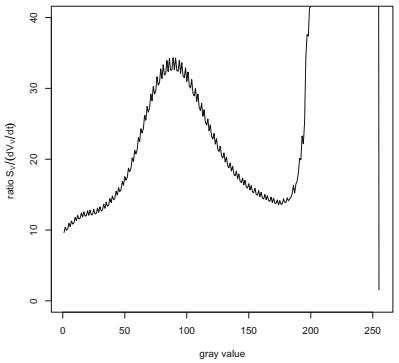

(c) Ratio of S_V and dV_V/dt

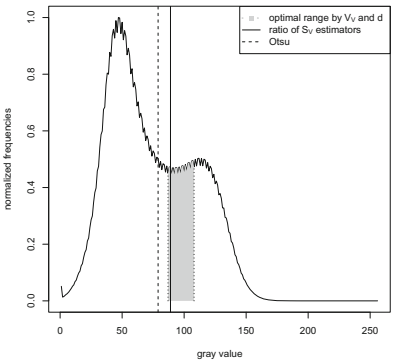

(d) Gray value histogram

Fig. 5. Characteristics as functions of gray value threshold for the glass fiber reinforced polymer sample. The known fiber thickness $d = 16\mu$m and the known fiber volume fraction $V_V = 35\%$ yield an interval of reasonable thresholds. Otsu's threshold (79) lies left of this interval, while the threshold defined by the mode of the ratio of S_V and dV_V/dt (89) lies well within.

The fiber weight content of the material is 60 %, resulting in an expected fiber volume fraction of 35 %. The image quality is very good, nevertheless it is impossible to segment the fiber system such that both the known fiber volume fraction and the known fiber thickness are perfectly fit. We therefore use the approach introduced above to find a good trade off between these two targets.

Note, that the noise in the plots is caused by the preprocessing of spreading the original 16bit image data to 8bit data.

Our numerical experiments deviated from the predictions derived from the Steiner formula, namely that the ratio between specific surface and first deriva-

(a) Region of slice through image binarized using Otsu's threshold

(b) Region of slice through image binarized using derived threshold

Fig. 6. Section through the thresholded images of the glass fiber reinforced polymer sample (detail of 4b). The resulting images are similar, note, that the fibers in some bundles are slightly better separated in 6b.

tive of the volume density should be one. We attribute this to discretization effects. Nevertheless, the surface density based threshold selection rule proposed in the present paper yields very promising results and we expect this method to be useful for segmentation of a wide range of microstructures.

5 Discussion

In this paper, we described an efficient algorithm for calculating the intrinsic volumes for each possible gray value threshold in an integer valued image and demonstrated two of its possible applications. Namely, the method can be used to derive efficiently the Minkowski functions of parallel body of a structure when applied to the Euclidean distance transformed image. Also, it can be used to find the global gray value threshold yielding the best agreement of the segmentation result with pre-known geometric characteristics of the structure.

Our algorithm is of linear complexity in the number of pixels. Even more important are the two other features: It works purely locally on the image and requires fixed memory space, independent of the size of the original image. This is extremely valuable, as with growing flat-panel detectors, alternative scanning geometries like helical (or spiral) computed tomography 3D image data reach sizes larger than 100GB.

References

1. Stoyan, D., Kendall, W.S., Mecke, J.: Stochastic Geometry and its Applications, 2nd edn. Wiley, Chichester (1995)

2. Schneider, R., Weil, W.: Stochastic and Integral Geometry. Probability and Its Applications. Springer, Heidelberg (2008)
3. Ohser, J., Redenbach, C., Schladitz, K.: Mesh free estimation of the structure model index. Image Analysis and Stereology 28(3), 179–186 (2009)
4. Schladitz, K., Redenbach, C., Sych, T., Godehardt, M.: Model based estimation of geometric characteristics of open foams. Methodology and Computing in Applied Probability, pp. 1011–1032 (2012)
5. Vogel, H.J.: Morphological determination of pore connectivity as a function of pore size using serial sections. European Journal of Soil Science 48(3), 365–377 (1997)
6. Mecke, K.: Additivity, convexity, and beyond: Application of minkowski functionals in statistical physics. In: Mecke, K.R., Stoyan, D. (eds.) Statistical Physics and Spatial Statistics. LNP, vol. 554, pp. 111–184. Springer, Heidelberg (2000)
7. Ohser, J., Nagel, W., Schladitz, K.: Miles formulae for Boolean models observed on lattices. Image Anal. Stereol. 28(2), 77–92 (2009)
8. Ohser, J., Schladitz, K.: 3d Images of Materials Structures – Processing and Analysis. Wiley VCH, Weinheim (2009)
9. Otsu, N.: A threshold selection method from gray level histograms. IEEE Trans. Systems, Man and Cybernetics 9, 62–66 (1979)
10. Ridler, T., Calvard, S.: Picture thresholding using an iterative selection method. IEEE Transactions on Systems, Man and Cybernetics 8(8), 630–632 (1978)
11. Schladitz, K., Ohser, J., Nagel, W.: Measurement of intrinsic volumes of sets observed on lattices. In: Kuba, A., Nyúl, L.G., Palágyi, K. (eds.) DGCI 2006. LNCS, vol. 4245, pp. 247–258. Springer, Heidelberg (2006)
12. Freitag, J., Wilhelms, F., Kipfstuhl, S.: Microstructure-dependent densification of polar firn derived from x-ray microtomography. Journal of Glaciology 50(169), 243–250 (2004)
13. Freitag, J., Kipfstuhl, S., Faria, S.H.: The connectivity of crystallite agglomerates in low-density firn at Kohnen station, Dronning Maud land, Antarctica. Ann. Glaciol. 49, 114–120 (2008)
14. Redenbach, C., Särkkä, A., Freitag, J., Schladitz, K.: Anisotropy analysis of pressed point processes. Advances in Statistical Analysis 93(3), 237–261 (2009)
15. Kronenberger, M., Wirjadi, O., Freitag, J., Hagen, H.: Gaussian curvature using fundamental forms for binary voxel data. Graphical Models (accepted, 2015)
16. Wirjadi, O., Godehardt, M., Schladitz, K., Wagner, B., Rack, A., Gurka, M., Nissle, S., Noll, A.: Characterization of multilayer structures in fiber reinforced polymer employing synchrotron and laboratory X-ray CT. International Journal of Materials Research 105(7), 645–654 (2014)